A LETTERS JOURNAL EXPLORING
THE FRONTIERS OF PHYSICS

OFFPRINT

On the dependency of friction on load: Theory and experiment

O. M. Braun, B. Steenwyk, A. Warhadpande and B. N. J. Persson

EPL, **113** (2016) 56002

A LETTERS JOURNAL EXPLORING
THE FRONTIERS OF PHYSICS

March 2016

EPL, **113** (2016) 56002
doi: 10.1209/0295-5075/113/56002

www.epljournal.org

On the dependency of friction on load: Theory and experiment

O. M. BRAUN[1,2], B. STEENWYK[3], A. WARHADPANDE[3] and B. N. J. PERSSON[2,4]

[1] *Institute of Physics, National Academy of Sciences of Ukraine - 03028 Kiev, Ukraine*
[2] *PGI, FZ-Jülich - 52425 Jülich, Germany, EU*
[3] *Bridgestone Americas Tire Operations - 10 E Firestone Blvd., Akron, OH 44317, USA*
[4] *Multiscale Consulting - Wolfshovener Straße 2, 52428 Jülich, Germany, EU*[(a)]

received 19 January 2016; accepted in final form 3 March 2016
published online 21 March 2016

PACS 68.35.Ct – Interface structure and roughness
PACS 46.55.+d – Tribology and mechanical contacts

Abstract – In rubber friction studies it is often observed that the kinetic friction coefficient depends on the nominal contact pressure. This is usually due to frictional heating, which softens the rubber, increases the area of contact, and (in most cases) reduces the viscoelastic contribution to the friction. In this paper we present experimental results showing that the rubber friction also depends on the nominal contact pressure at such low sliding speed that frictional heating is negligible. This effect has important implications for rubber sliding dynamics, *e.g.*, in the context of the tire-road grip. We attribute this effect to the viscoelastic coupling between the macroasperity contact regions, and present a simple earthquakelike model and numerical simulations supporting this picture. The mechanism for the dependency of the friction coefficient on the load considered is very general, and is relevant for non-rubber materials as well.

Introduction. – The Coulomb friction law states that the friction force $F_\mathrm{f} = \mu F_\mathrm{N}$ is proportional to the normal force or load F_N, and is found to hold remarkable well in many practical applications [1,2]. For elastic solids with nominally flat but randomly rough surfaces, contact mechanics theories and numerical simulations show that the contact area A is proportional to the nominal contact pressure $p_0 = F_\mathrm{N}/A_0$, where A_0 is the nominal contact area [3–10]. If it is assumed that a characteristic frictional shear stress τ_f acts in the area of real contact, then the friction coefficient $\mu = \tau_\mathrm{f} A/(p_0 A_0)$ will be independent of the pressure p_0, *i.e.*, independent of the normal load $F_\mathrm{N} = p_0 A_0$. There are many reason why the Coulomb friction law may fail, and in this letter we discuss a fundamental and very general mechanism, which is also very important for rubber friction, *e.g.*, for the friction between tires and road surfaces.

In the following we consider surfaces which are nominally flat but exhibit roughness at length scales much shorter than the linear size L of the surface. Such surfaces have surface roughness power spectra with a roll-off region for small wave numbers [11]. When such surfaces are observed at low magnification one observes only the most long wavelength part of the surface roughness, and the contact appears to consist of randomly distributed *macroasperity* contact regions [4]. When a macroasperity contact region is observed at higher magnification, shorter wavelength roughness is observed and the macroasperity contact region breaks up into smaller *microasperity* contact regions.

Contact mechanics studies show that with increasing pressure p_0, existing contact areas grow and new contact areas form in such a way that the (normalized) interfacial stress distribution, and also the size distribution of contact spots, are independent of the squeezing pressure [3–6]. When this is the case the macroscopic friction force will be proportional to the normal force even when the friction force acting on the asperity contact regions at the smallest length scale depends non-linearly on the asperity contact area, as often found to be the case in nanoscale sliding friction experiments [12,13]. In this case the only thing which could influence the sliding friction is the concentration (a real density) of macroasperity contact regions, which increases proportional to p_0. In ref. [14] it was suggested that the lateral coupling between the macroasperity contact regions may result in a dependency of the friction coefficient on the load.

In this letter we present a very simple model for the elastic (or viscoelastic) coupling between the macroasperity contact regions, and we show that the lateral coupling

(a) www.multiscaleconsulting.com

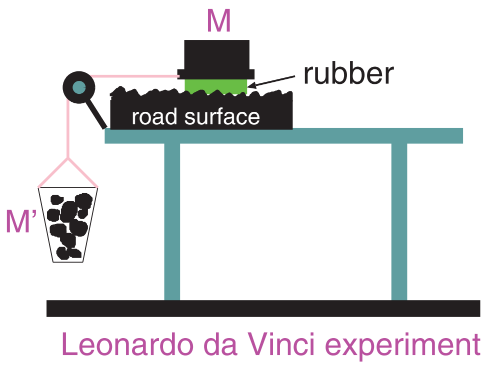

Fig. 1: (Color online) Simple friction tester (schematic) used for obtaining the friction coefficient $\mu = M'/M$ as a function of the sliding speed. The sliding distance is measured using a distance sensor and the sliding velocity v obtained by dividing the sliding distance with the sliding time. This set-up can only measure the friction coefficient on the branch of the $\mu(v)$-curve where the friction coefficient increases with increasing sliding speed v.

between the contact regions influences the stick-slip dynamics of the contact regions. This results in a dependency of the friction coefficient on the load, similarly to what we have observed in rubber friction experiments [14,15].

Experimental. – At low sliding speeds, when the frictional heating is negligible, many experiments show that the rubber friction coefficient on rough surfaces is approximately independent of the normal load which we too observe in most cases. However, we have found that close to the first maximum (as a function of increasing sliding speed v) of the $\mu(v)$ friction curve (the first maximum is due to the adhesive interaction between the rubber and the road surface in the area of real contact [15,16]), the friction coefficient decreases slightly with increasing nominal contact pressure. The friction coefficient at this maximum is very important for tire dynamics —it acts as an effective static friction coefficient (the slip velocities before the first maximum of $\mu(v)$ are very small, and can be neglected in most tire applications [17,18]).

We have studied rubber friction for tread rubber compounds sliding against concrete and asphalt road surfaces. The measurements were performed using the Leonardo da Vinci set-up shown in fig. 1. The slider consists of two rubber blocks glued to a wood plate (with a rubber block thickness ~ 0.5 cm typically larger than the diameter of the macroasperity contact regions). This simple friction tester can be used for obtaining the friction coefficient $\mu = M'/M$ as a function of the sliding speed. The sliding distance is measured using a distance sensor, and the sliding velocity obtained by dividing the sliding distance with the sliding time. This set-up can only measure the steady-state friction coefficient on the branch of the $\mu(v)$-curve where the friction coefficient increases with increasing sliding speed v. Thus, if $v = v_{\max}$ denote the velocity where the $\mu(v)$-curve has its first maximum, then in figs. 2 and 3 below, the highest velocity data points correspond to the sliding speed $v = v_{\max}$.

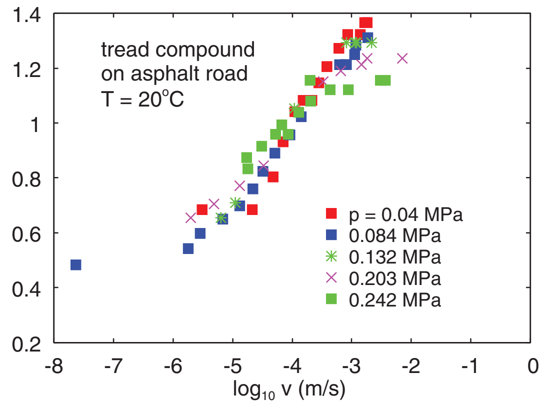

Fig. 2: (Color online) The measured friction coefficient as a function of the sliding speed for a rubber compound on an asphalt road surface. The background temperature is $T_0 = 20\,^\circ$C, and the nominal contact pressure is indicated in the figure.

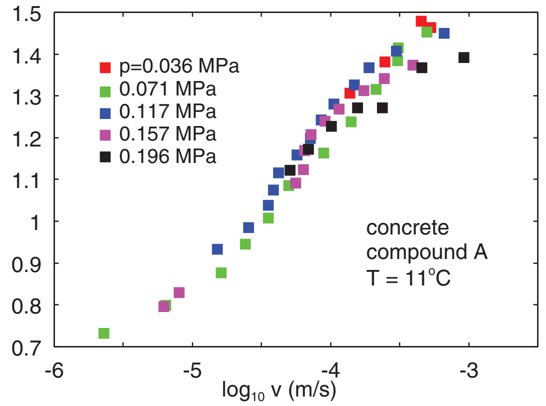

Fig. 3: (Color online) The measured friction coefficient as a function of the sliding speed for a rubber compound on a concrete road surface. The background temperature is $T_0 = 11\,^\circ$C, and the nominal contact pressure is indicated in the figure.

Figure 2 shows the measured friction coefficient as a function of the sliding speed for a rubber tread compound on an asphalt road surface. The results are for the background temperature $T_0 = 20\,^\circ$C, and for several values of the nominal contact pressure indicated in the figure. Note that the maximum of the friction coefficient decreases with increasing nominal contact pressure. At the same time the friction coefficient for lower velocities is the same in all cases within the accuracy of the measurements.

Figure 3 shows the measured friction coefficient as a function of the sliding speed for a rubber tread compound on a concrete road surface. The results are for the background temperature $T_0 = 11\,^\circ$C, and for several nominal contact pressure. Note again that the maximum of the friction coefficient decreases with increasing nominal contact pressure.

Figures 2 and 3 show that there is a big spread in the measured friction data. We believe this is due to the influence of surface contamination on the adhesive contribution to the friction. This is particularly true close to the maximum in $\mu(v)$ where the measured data depends on how clean the surface is., *e.g.*, how long the surface has been in the normal atmosphere after the surface was cleaned in soap-water. We note that the adhesive contribution to $\mu(v)$ most likely involves the (temporary) binding of rubber molecules to the substrate which is sensitive to even sub-monolayer surface contamination. However, we have studied many more systems than shown in the present paper, and as the nominal contact pressure increases we always observed a systematic reduction in the friction coefficient close to the maximum of $\mu(v)$, while there is no systematic pressure dependence of the friction coefficient well away from the maximum.

Qualitative discussion. – A tentative explanation for the observations above is as follows [14]. For velocities $v \ll v_{\max}$ the rubber in (almost) all macroasperity contact regions slip relative to the substrate with the same velocity v as the upper surface of the rubber block. In that case the elastic (or rather viscoelastic) coupling between the rubber macroasperity contact regions is not changing in time, and it is basically irrelevant for the friction. Now, for velocities $v > v_{\max}$ the rubber friction decreases with increasing sliding speed. In the present case where the driving force is constant, this results in an unstable branch of the $\mu(v)$-curve, where the rubber block accelerates.

If instead the upper surface of the block would be rigidly driven with a constant velocity $v > v_{\max}$, the bottom surface of the block would perform stick-slip motion. But with the same argument one expects the rubber in the macroasperity contact regions to perform stick-slip motion for $v > v_{\max}$. However, due to the stochastic fluctuations in the nature of the macroasperity contact regions (*e.g.*, due to local fluctuations in the roughness or surface contamination) one expects not a sharp onset velocity for stick-slip motion at the macroasperity level, but a distribution of onset velocities. Thus we expect that close to the friction maximum, but for $v < v_{\max}$, some contact regions will perform stick-slip motion. In this case the motion of a macroasperity contact region depends on the motion of the other macroasperity contact regions. Thus, we expect some correlation in the local stick-slip events when the velocity is close to the point where the friction coefficient is maximal. For example, if the rubber in a macroasperity contact region slips into a state where the shear force acting on it vanishes, the tangential force lost in this contact region will distribute itself on the other rubber macroasperity contact regions, where the shear stress now may increase to the point of resulting in local slip, and so on. Clearly, this lateral coupling, and the way the stress redistributes itself in response to a local slip at a macroasperity contact region, will depend on the average separation between the macroasperity contact regions, and hence on the concentration of the macroasperity contact regions, which increases with increasing nominal contact pressure.

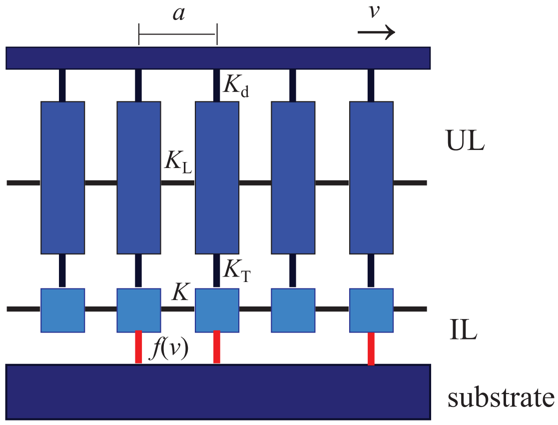

Fig. 4: (Color online) The model. The upper layer (UL) is split in rigid blocks of size $a \times a \times N_L a$ connected by springs of the elastic constant K_L. The interface layer (IL) is split in rigid blocks of size $a \times a \times a$ connected by springs of the elastic constant K. The UL and IL are coupled by springs of the elastic constant K_T. The IL is connected with the rigid bottom block (substrate) by frictional contacts (see eq. (1)). The UL is driven with the velocity v through springs of the elastic constant K_d.

We now present a simple analytical model to study in greater detail the mechanism discussed above, and we will show that the lateral coupling between the macroasperity contact regions gives rise to a friction coefficient $\mu(v)$ which depends on the load or normal force for v close to $v_{\max}$.

Theory modeling. – We now discuss why the friction coefficient in figs. 2 and 3 depends on the nominal contact pressure for sliding speeds close to $v = v_{\max}$, where the friction coefficient has a local maximum. We assume that the contact area is proportional to the nominal contact pressure p_0, and that with increasing pressure p_0, existing contact areas grow and new contact areas form in such a way that the (normalized) interfacial stress distribution, and also the size distribution of contact spots are independent of the squeezing pressure. (Strictly speaking, this assumption only holds for an infinite system, but should be approximately true also in most practical applications.) In this case the only thing which could influence the sliding friction is the concentration (a real density) of macroasperity contact regions which increases proportional to p_0.

Unfortunately, an exact consideration of the elastic coupling between the macroasperity contact regions is possible only within a three-dimensional model, which require very large computational time for system sizes of interest. In this first study we therefore instead use a simple one-dimensional two-chain model of the slider (see fig. 4), which should be enough to demonstrate if the lateral coupling between the macroasperity contact regions can generate a load dependency of the friction coefficient.

Our model is similar to the Burridge and Knopoff spring-block model [19] used to study some aspects of earthquake dynamics and boundary lubrication [20]. In this model the top block (the slider) is coupled with the bottom block (substrate), assumed to be rigid and fixed, by a set of frictional contacts. In refs. [21,22] this model was extended in order to incorporate elasticity of the slider in an approximate way.

The model is shown schematically in fig. 4. The bottom chain consists of rigid a^3-cubes coupled by springs $K = Ea$, where E is the slider Young modulus, and also coupled by frictional contacts with the base; it describes the macroasperity contact regions, here referred to as the "interface" layer (IL).

The other part of the slider is modeled as a chain of parallelepipeds of height $N_\mathrm{L}a$ coupled by springs $K_\mathrm{L} = N_\mathrm{L}Ea$; we call it the upper layer (UL). The UL and IL are coupled by the set of N transverse springs $K_\mathrm{T} = Ga/N_\mathrm{L}$, where $G = E/[2(1+\nu)]$ is the shear modulus and ν is the slider Poisson ratio. The UL plays the role of a reservoir, where the elastic energy is stored and partially released during sliding. Finally, we attach springs K_d to the top boundary of UL and drive the spring ends with a velocity v. Along the chains we use periodic boundary conditions.

The model parameters for the rubber slider are the following. The IL consists of $N = 301$ or 1001 blocks (a^3-cubes), each of linear size $a = 0.1\,\mathrm{mm}$ and mass $m = \rho a^3 = 10^{-9}\,\mathrm{kg}$, where $\rho = 10^3\,\mathrm{kg/m^3}$ is the rubber mass density. The rubber has a Young modulus $E = 10\,\mathrm{MPa}$ and a Poisson ratio $\nu = 0.5$, so that the springs between the cubes has an elastic constant $K = 10^3\,\mathrm{N/m}$.

The UL consists of parallelepipeds of height $N_\mathrm{L} = 5$ (so that their masses are $N_\mathrm{L}m$). The UL is moved through springs of the elastic constant $K_\mathrm{d} = K/[2(1+\nu)]$ attached to its top and driven with a velocity v. Between the nearest-neighboring blocks i and j we added the viscous damping force $f_{ij} = -m\eta(v_i - v_j)$ with the damping coefficient $\eta = 0.3\omega_0$, where $\omega_0 = (K/m)^{1/2} = 10^6\,\mathrm{s}^{-1}$ is the characteristic frequency of the slider, so that the system dynamics is underdamped.

The slider is coupled with the substrate by $N_\mathrm{c} = \theta N$ frictional contacts with a random spatial distribution. As discussed above, for a contact of rough surfaces the dimensionless parameter θ is directly proportional to the load. The force acting on the i'th IL's block, to which the contact is attached, depends on the block velocity v_i as [15]

$$f(v_i, v_i^*) = \varepsilon f_0 \exp(-c\xi_i)\mathrm{sign}(v_i) + m\eta_\mathrm{c} v_i, \quad (1a)$$

$$\xi_i = \left[\log_{10}\left(|v_i|/v_i^*\right)\right]^2, \quad (1b)$$

where $f_0 = a^2\tau_\mathrm{f}$, $\tau_\mathrm{f} = 6.5\times10^6\,\mathrm{Pa}$ and $c = 0.1$, and the parameters v_i^* are randomly distributed around the value $v_0 = 1\,\mathrm{mm/s}$ [15] (in detail, the values $\log_{10} v_i^*$ are uniformly distributed within the interval $[\log_{10} v_0 - \delta, \log_{10} v_0 + \delta]$ with $\delta = 0.5$). The function $f(v, v_0)$, eq. (1), is shown in fig. 5 for different values of the contact's damping η_c.

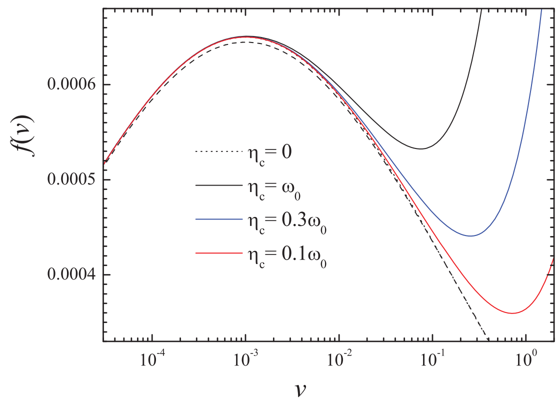

Fig. 5: (Color online) The function $f(v, v_0)$, eq. (1), for different values of the damping coefficient $\eta_\mathrm{c} = 0$ (dotted line), $\eta_\mathrm{c} = \omega_0$ (solid black line), $\eta_\mathrm{c} = 0.3\omega_0$ (blue line) and $\eta_\mathrm{c} = 0.1\omega_0$ (red line). The dashed curve shows the force $\langle f(v, v_i)\rangle = N_\mathrm{c}^{-1}\sum_{i=1}^{N_\mathrm{c}} f(v, v_i)$ averaged over all contacts for $N = 1001$ and $\theta = 1$.

The "scaling" parameter ε in eq. (1) was introduced because of the following technical problem [23]. The characteristic time scale of the slider is $\tau_0 = 2\pi/\omega_0 \approx 6.3\times10^{-6}\,\mathrm{s}$, while the characteristic time scale of the frictional contacts is $\tau_\mathrm{c} = v_0 m/f_0 \sim 10^{-12}\,\mathrm{s}$ which is more than six orders of magnitude smaller. Using the value $\varepsilon = 10^{-2}$ in eq. (1), we were able to simulate the system within a reasonable computer time (of course, we checked that changing of ε does not modify our results, at least qualitatively).

During the simulation we saved the total driving force $f_\mathrm{d}(t) = N^{-1}\sum_{i=1}^{N} K_\mathrm{d}[v_\mathrm{d}t - X_i(t)]$, where $X_i(t)$ is the coordinate of the i-th UL's block, and then calculated the parameter $\mu^* = \langle f_\mathrm{d}(t)\rangle/(\varepsilon f_0\theta)$ for the steady sliding. Since θ is proportional to the normal load, μ^* is directly proportional to the friction coefficient. The results are presented in fig. 6. For a lower driving velocity $v_{\mathrm{d}2} = 3\times10^{-4}\,\mathrm{m/s}$ the friction is almost independent of load, while for $v_{\mathrm{d}1} = v_0 = 10^{-3}\,\mathrm{m/s}$ the friction may decrease by more than 20% when the load grows, in good agreement with the experiment.

Analyzing the simulation results in more detail, we found the following explanation of this effect. Let v be the velocity of the drive. A single (isolated) contact i moves with a constant velocity v if $v < v_i^*$, and hence it experiences the constant friction force $f(v, v_i^*)$. However, if $v > v_i^*$ for the given contact, its motion becomes unstable, and the contact undergoes stick-slip motion. In the latter case, the contact accelerates during slip, and the force drops, so the averaged force from this contact is lower than $f(v, v_i^*)$; the larger the effect is, the smaller the damping parameter η_c is. For a set of non-interacting contacts, the driving force in the steady state is approximately equal to the sum of the forces from all contacts, and thus slightly smaller than $\langle f(v, v_i^*)\rangle$ because some contacts with $v_i^* < v$ undergo stick-slip. This situation

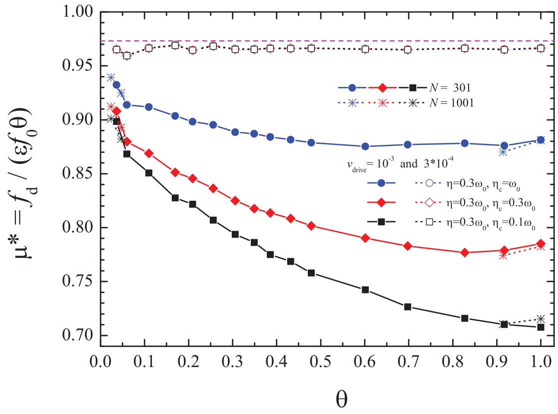

Fig. 6: (Color online) Dependence μ^* *vs.* θ for three values of the contact damping $\eta_c = \omega_0$ (blue circles), $\eta_c = 0.3\omega_0$ (red diamonds) and $\eta_c = 0.1\omega_0$ (black squares), and for two values of the driving velocity $v_{d1} = v_0 = 10^{-3}$ m/s (solid symbols) and $v_{d2} = 0.3v_0 = 3\times10^{-4}$ m/s (open symbols; the dashed horizontal line shows $f(v_{d2}, v_0)/(\varepsilon f_0 \theta)$). Stars are for $N = 1001$.

corresponds to the $\theta \to 0$ limit (low load), when the contacts are far away from each other. However, at large θ (load) some contacts occur close to one another, and if one of them undergoes stick-slip, it will stimulate the neighboring contacts to stick-slip as well —the number of stick-slip contacts increases with θ, and the total friction force decreases.

The stick-slip of the macroasperity contact regions should manifest itself in the power spectrum of the block velocity, and in the acoustic power spectrum, so studying these quantities should be one way to test the hypothesis presented above.

Summary and conclusion. – In this paper we presented experimental results showing that the rubber friction coefficient $\mu(v)$, in a narrow velocity region around the velocity where $\mu(v)$ is maximal, depends on the nominal contact pressure p_0, even when the sliding speed is so low that frictional heating is unimportant. We attribute this effect to the (viscoelastic) coupling between the macroasperity contact regions. We have presented a simple model which shows that the lateral coupling between the macroasperity contact regions can enhance the stick-slip of the contact regions. Since the average distance between two nearby macroasperity contact region decreases when the load increases, the lateral coupling increases, and the friction coefficient decreases, as the load increases.

The mechanism for the dependency of the friction coefficient on the load considered in this paper is very general, and is also relevant for non-rubber materials. We plan to perform studies on more realistic 3D systems to test if the predictions presented in this paper holds also in a more accurate treatment of the problem.

* * *

The research work was performed within a Reinhart-Koselleck project funded by the Deutsche Forschungsgemeinschaft (DFG). We would like to thank DFG for the project support under the reference German Research Foundation DFG-Grant: MU 1225/36-1. The research work was also supported by the DFG-grant: PE 807/10-1. This work is supported in part by COST Action MP1303.

REFERENCES

[1] Rabinowicz E., *Friction and Wear of Materials* (Wiley) 1995.

[2] Persson B. N. J., *Sliding Friction: Physical Principles and Applications* (Springer-Verlag, Berlin) 2000.

[3] Persson B. N. J., *J. Chem. Phys.*, **115** (2001) 3840.

[4] Persson B. N. J., *Surf. Sci. Rep.*, **61** (2006) 201.

[5] Hyun S., Pei L., Molinari J. F. and Robbins M. O., *Phys. Rev. E*, **70** (2004) 026117.

[6] Campana C. and Müser M. H., *EPL*, **77** (2007) 38005.

[7] Yastrebova V. A., Anciaux G. and Molinari J. F., *Int. J. Solids Struct.*, **52** (2015) 83.

[8] Persson B. N. J., Sivebaek I. M., Samoilov V. N., Zhao K., Volokitin A. I. and Zhang Z., *J. Phys.: Condens. Matter*, **20** (2008) 395006.

[9] Pastewka L. and Robbins M. O., *Proc. Natl. Acad. Sci. U.S.A.*, **111** (2014) 3298.

[10] Persson B. N. J. and Scaraggi M., *J. Chem. Phys.*, **141** (2014) 124701.

[11] Persson B. N. J., *Tribol. Lett.*, **54** (2014) 99.

[12] Müser M. H., *Europhys. Lett.*, **66** (2004) 97.

[13] Dietzel D., Feldmann M., Schwarz U. D., Fuchs H. and Schirmeisen A., *Phys. Rev. Lett.*, **111** (2013) 235502.

[14] Fortunato G., Ciaravola V., Furno A., Scaraggi M., Lorenz B. and Persson B. N. J., submitted to *Tire Sci. Technol.* (2015), see also arXiv:1512.01359.

[15] Lorenz B., Oh Y. R., Nam S. K., Jeon S. H. and Persson B. N. J., *J. Chem. Phys.*, **142** (2015) 194701.

[16] Grosch K. A., *Proc. R. Soc. London, Ser. A*, **274** (1963) 21.

[17] Persson B. N. J., *J. Phys.: Condens. Matter*, **23** (2011) 015003.

[18] Selig M., Lorenz B., Henrichmöller D., Schmidt K., Ball A. and Persson B. N. J., *Tire Sci. Technol.*, **42** (2015) 216.

[19] Burridge R. and Knopoff L., *Bull. Seismol. Soc. Am.*, **57** (1967) 341.

[20] Persson B. N. J., *Phys. Rev. B*, **51** (1995) 13568.

[21] Braun O. M. and Tosatti E., *Phys. Rev. E*, **90** (2014) 032403.

[22] Braun O. M. and Scheibert J., *Tribol. Lett.*, **56** (2014) 553.

[23] Braun O. M. and Tosatti E., *Philos. Mag.*, **91** (2011) 3253.